私立東海大學

資訊工程研究所

碩士論文

指導教授：黃育仁 博士

電腦斷層掃描影像在延遲相上左心室心肌區域切割

Left Ventricular Myocardium Segmentation on Delayed Phase of Multi-detector Row Computed Tomography

研究生：劉柏廷

中　華　民　國　一　百　年　六　月

摘要

左心室心肌容量的異常與許多心血臟疾病息息相關，因此左心室容量是一個用來診斷心血管疾病的重要參考。為了協助醫師與放射線師評估心室的容積，本研究提出一個在延遲相電腦斷層影像自動找出左心室的心肌輪廓並且計算其容積方法。由於相鄰的影像有一定的相似性。因此、切割出第一張 Leading slice 後，即可用此結果切割相鄰的影像。首先利用動脈相的輪廓、mean shift 與門檻值找出大致上的心肌區域，接著利用區域成長與凸包(convex hull)演算法來找出心內膜區域，最後使用形態學與心肌寬度大致相同的這個特性，找出心外膜並且計算其心肌容積，如此便可以得到 Leading slice 的結果。再使用 Leading slice 切割相鄰影像，並將結果與兩位熟練專家所描繪的輪廓進行比較，實驗結果證實此系統可得到相當高的相似度(similarity index, SI)，此方法可以用於自動描繪出心肌輪廓，並且計算其面積。

關鍵字：電腦斷層；心肌輪廓；影像切割；心肌容積；缺血性心臟病

ABSTRACT

Many cardiac diseases are related to volume of cardiac left ventricle (LV). Thus volume of cardiac LV is important information to diagnose ischemic heart diseases. In order to assist radiologists and physicians to estimate the LV volume, this study proposed an automatic segmentation method to contour the myocardial region in delayed phase of multi-detector row computed tomography (MDCT) imaging and then compute the volume of cardiac LV myocardium. The proposed method performs roughly myocardium base on threshold and contour that contour from artery phase. The endocardium would obtain after the methods that region growing, Convex-hull was used. Finally, the width similar properties within myocardial region and the morphology operators are used to obtain the whole LV myocardial volume. Compared with the contours manually delineated by two experienced experts, the automatic contouring results from computer simulation reveal that the proposed method always identifies similar contours as that obtained by the manual sketching.

Keywords: multi-detector row computed tomography; myocardium contouring; image segmentation; myocardial volume; ischemic heart disease

INDEX

LIST OF FIGURES

LIST OF TABLES

CHAPTER 1 INTRODUCTION

Abnormal volume of cardiac left ventricle (LV) would cause ischemic heart disease. Ischemic heart disease can reduce the cardiac output and cause heart failure or even death if severe. Due to early diagnosing ischemic heart disease is very important, the volume of cardiac LV become a valuable feature for radiologists and physicians to make decision[1]. Cardiac multi-detector row computer tomography (MDCT) has been shown as a promising tool in the diagnosis of ischemic heart disease. The myocardial variation of MDCT is clinically significant due to thinning of the myocardium of LV probably denotes myocardial infarction. Measuring myocardium volumes from the MDCT images could help to determine the infarction volume of LV by both arterial and delayed phases.

However, a complete scans of cardiac were approximately fifteen to thirty serial slices. The original MDCT imaging on delayed phase was in a low contrast and contains numerous noises, as shown in Fig. 1. Sketching myocardium of LV manually was very time-consuming for radiologists. Moreover, the results might increase the error due to tiring to contour the myocardial boundaries[2]. For conserving the time of sketching the LV myocardium, this study developed a segmentation scheme to obtain the myocardial contours on delayed phase of MDCT imaging and then to estimate the volume of cardiac LV myocardium.

Many researches nowadays developed useful segmentation algorithms which performed specific model or compose method[3]. Due to the myocardial region and other tissues hold a similar intensity, the segmentation for the cardiac LV myocardium on delayed phase of MDCT is a difficult task. The previous algorithms might be used in arterial phase of CT imaging but worked poorly in delayed phase of MDCT. Moreover, the segmentation methods performed on each MDCT slice individually, without employ the relationship in the adjacent slices. Figure 2 illustrates the tissues which are outside of myocardial but present similar intensity to the myocardial region.

In general, the conventional image segmentation could categorize into intensity-based, shape-based and deformable-based methods. The region-based methods such as level-set[4,5], region growing[6] and watershed[7,8] algorithms have been shown to be practical methods for tissue segmentation in medical imaging. However, original images in delayed phase of MDCT are in a low contrast and always comprise quantities of noises. Directly applying the region-based methods for extracting LV myocardium constantly obtained unsatisfied segmentation results. The aim of this study is to develop an efficient segmentation method to overcome the task. Firstly, the automatic thresholding method[9,10] was utilized to locate rough myocardial region from the MDCT imaging. Then the region growing method with convex-hull[11] finding algorithm was performed to exclude papillary muscle areas. Finally, the precise

LV myocardium region would obtain by using morphology operators[12] with width similar properties in myocardium area.

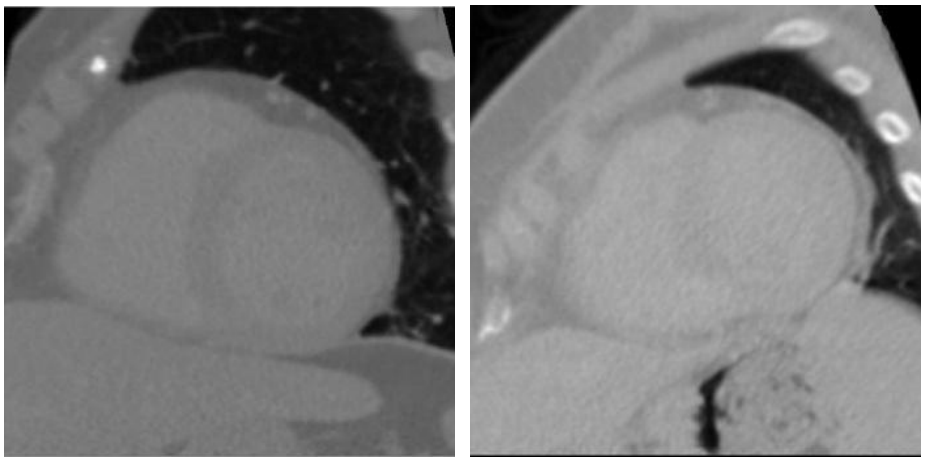

(a) (b)

Fig.1. Examples of the cardiac LV myocardium on delayed phase of MDCT imaging

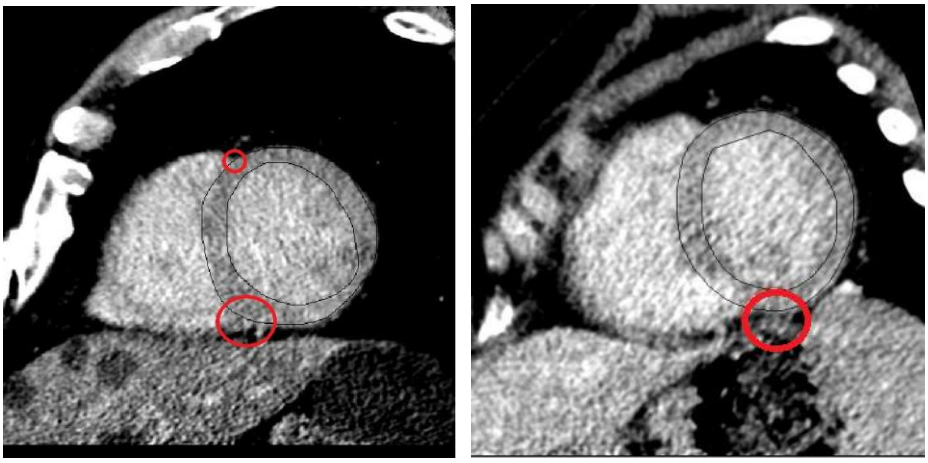

(a) (b)

Fig. 2. The tissues (the red ellipses) which are outside of LV myocardium; (a) and (b) correspond with Fig. 1(a) and (b), respectively. The outer contour was epicardium and inner contour was endocardium.

CHAPTER 2 MATERIALS

The experimental data of the MDCT images was from 27 healthy volunteers (from 40 to 80 years old) from the Taichung Veterans General Hospital. Data was acquired on 40 detector row MDCT (Brilliance 40; Philips, Best, the Netherlands) by senior physician. All scans were stored as DICOM format with 512 × 512 matrices. The pilot images were quantized into 12 bits (i.e. 4096 gray levels). Figure 3 illustrates the serial short axis images covering the entire LV had been created from apex of the heart. Thickness for short axis images was 5 mm. First five slices counting from the bottom are defined as apex (Apex), the sixth to tenth slices are defined as mid-ventricular level (MidV) and the remaining slices are defined as base (Base).

Any volunteer has approximately twenty image slices of LV. Each image slice was similar to the adjacent slices, thus the obtained result could offer a reference to the next adjacent slices when a myocardial region was segmented. By this way, myocardial region in all slices automatic generated after the f leading slice result was accomplished. Among the patients have apparent different in Base and Apex, and possibly not contain the myocardial region in those images. The MidV slices were always regular and obvious. Therefore, the proposed contouring method picked the middle of MidV images as leading slice. Let S_i, the i^{th} slice, was selected as the leading slice in an MDCT imaging. Since each image is similar to adjacent slices, after extracting the contours

from S_i, the obtained contours were utilized as the initial contours to segment the corresponding preceding slice S_{i-1} or the following slice S_{i+1}. However, if the extracted contour was unreasonable, the iterative contouring procedure in this study would be terminated.

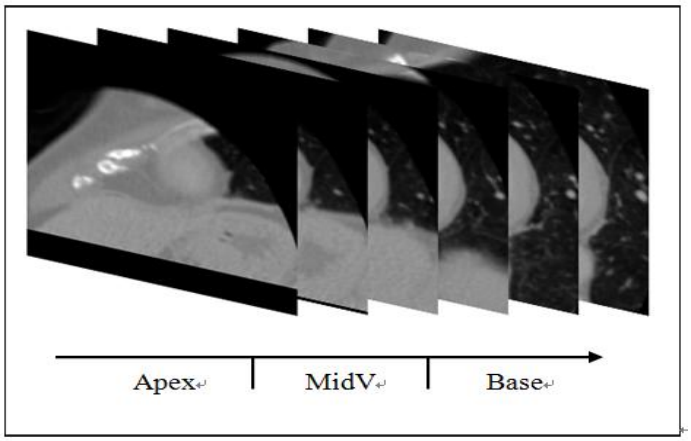

Fig. 3. The serial short axis images covering the entire LV had been created from apex of the heart.

CHAPTER 3 METHODS

Figure 4 presents a flowchart of proposed method that segments adjacent slices. The process would segment adjacent slices by forward slice until termination conditions was accomplished. Figure 5 presents a flowchart of the segmentation that includes the leading slice contouring, myocardium segmentation and extracted contour post-processing and completion validation checking. Due to the contour of leading slice is the groundwork for success in following slices segmentation, this study performed a two-pass procedure, i.e. full-automatic segmentation and semi-automatic segmentation, to prevent unreasonable contouring of the leading slice. A completion validation procedure checked the correctness of the obtained contours from the full-automatic segmentation. If the segmentation result was unsatisfying, the semi-automatic segmentation was activated to generate myocardium region of LV.

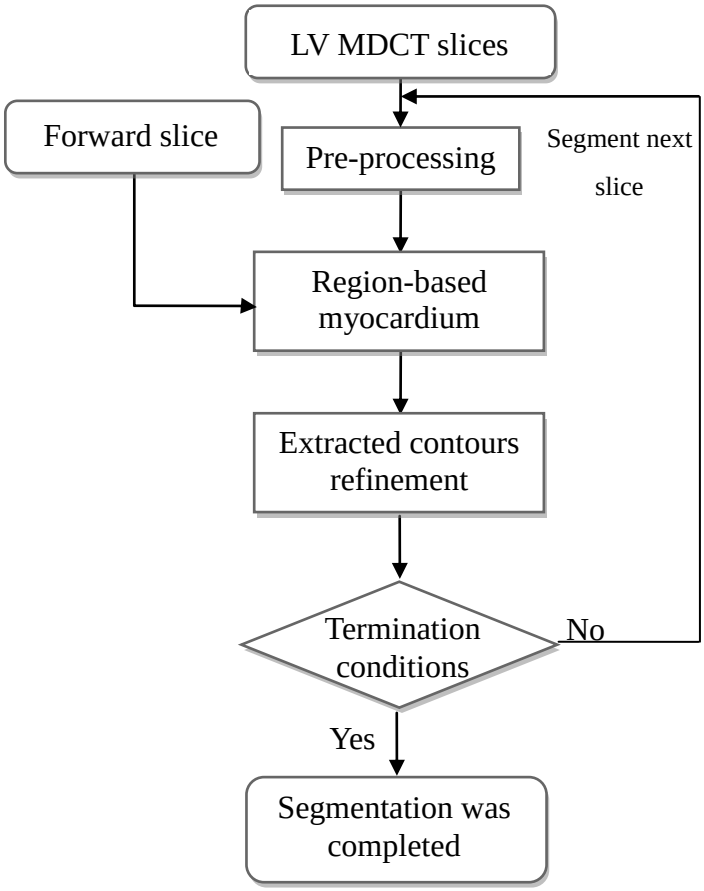

Fig. 4. The flowchart of segment slice by forward slice

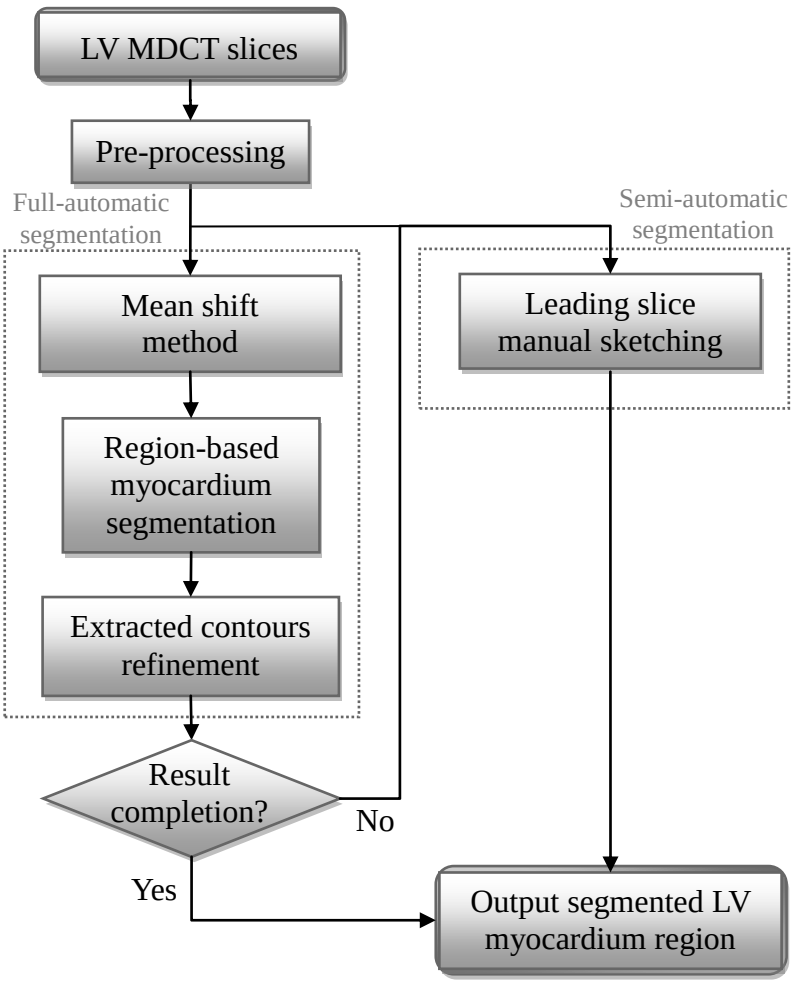

Fig. 5. The flowchart of segment leading slice

3.1 Pre-Processing

The original images of MDCT always comprise noises, preprocessing step was needed to reduce noises and enhance LV borders in the proposed method. Traditional de-nosing filters not only decrease noises, but also blur the sharp boundary of anatomical structures. Perona et al. proposed a linear-filter, i.e. anisotropic diffusion filter[13], to reduce noises and conserve the sharp boundaries. The anisotropic diffusion filter was employed to smooth myocardium of LV and to weaken the speck caused of

papillary muscle. The anisotropic diffusion according to the following equation:

$$\frac{\partial g(x,y,t)}{\partial t} = div(c\nabla g(x,y,t)), \quad (1)$$

where $g(x, y, t)$ is the resulted image at time t; x and y are the coordinates of two dimension. While $t=0$, $g(x, y, 0)$ is the initial image. The equation of anisotropic diffusion includes a variable, the conductance term, which can prevent edges from being smoothed:

$$c = e^{\frac{|\nabla g|^2}{2k^2}}, \quad (2)$$

where k is the parameter controlling the amount of diffusion near object edges. Figure 6 illustrates the preprocessed result of the proposed method.

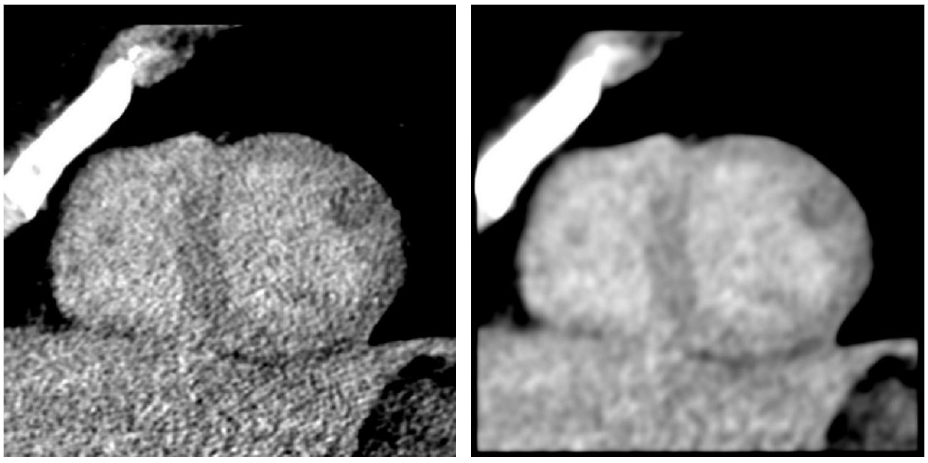

(a) (b)

Fig. 6. (a) An original image and (b) the preprocessed image

3.2 Leading Slice Contouring

The myocardium region of the leading slice should be obtained for adjacent slices segmentation. This study performed two leading slice contouring modes, i.e. manual sketching mode and automatic sketching mode. The manual sketching mode denoted physician manually sketched the myocardium contour on leading slice. Two experienced radiology physicians who were familiar with cardiac MDCT interpretations manually determined the contour of the myocardium. Moreover, this study developed an automatic version of leading slice contouring. The automatic sketching mode utilized the automatic generated contour of myocardium in arterial phase as contour of leading slice. Our previous work presents a hybrid segmentation method for left ventricular myocardium on arterial phase of MDCT imaging[14].

Due to myocardium imaging may be dissimilar between arterial phase and delay phase, as shown in Fig. 7. The contour in delay phases couldn't obtain to make used of arterial phases directly. The Mean shift method[15], Otsu algorithm[16], morphology operator and characteristic of myocardium were used to solved the problems about the distinct location and slice dimension. Employed capability of Mean shift could found the mass of region, the problem of location could be effectively solved. The inner of myocardium (equal endocardium) had higher gray-level intensity than around tissue. The Mean shift method could found the cluster that the mask had higher gray-level

intensity. Offset-vector from offset of mask was found after Mean shift, and correct endocardium was shifted former myocardium to rely on the offset-vector. Otsu algorithm was used on the region that including endocardium and epicardium after shifted by vector and used dilate of morphology operator with 3×3 structuring element. Added the characteristic of myocardium was used, the leading slice sketching was obtained through prior these step.

Mean-shift is a non-parametric feature-space analysis technique in computer vision and image processing, the method looks for the greater gray-level function given discrete data sampled from that function. This method is useful for detecting the modes of the density that greater gray-level is assembled. The procedure is an iterative and start with an initial estimate x. Let a kernel function $K(x_i - x)$ is given and determines the weight of nearby points for re-estimation of the mean. Typically the Gaussian kernel is used to evaluate the distance to the current estimate: $K(x_i - x) = e^{c\|x_i - x\|}$. The weighted mean of the density in the window determined by K is

$$m(X) = \frac{\sum_{x_i \in N(x)} \mathrm{K}(x_i - x) x_i}{\sum_{x_i \in N(x)} \mathrm{K}(x_i - x)}, \tag{3}$$

where $N(x)$ is the neighborhood of x, a set of points for which $K(x) \neq 0$.. The mean-shift algorithm now sets $x \leftarrow m(\mathbf{x})$, , and repeats the estimation until $m(x)$ converges to x. In this study, the initial x was contour of artery phase and offset- vector

was obtained after mean-shift. The offset-vector was displacement of myocardium between arterial phases and delay phases. The correct endocardium was shifted former myocardium to rely on the offset-vector with artery phase.

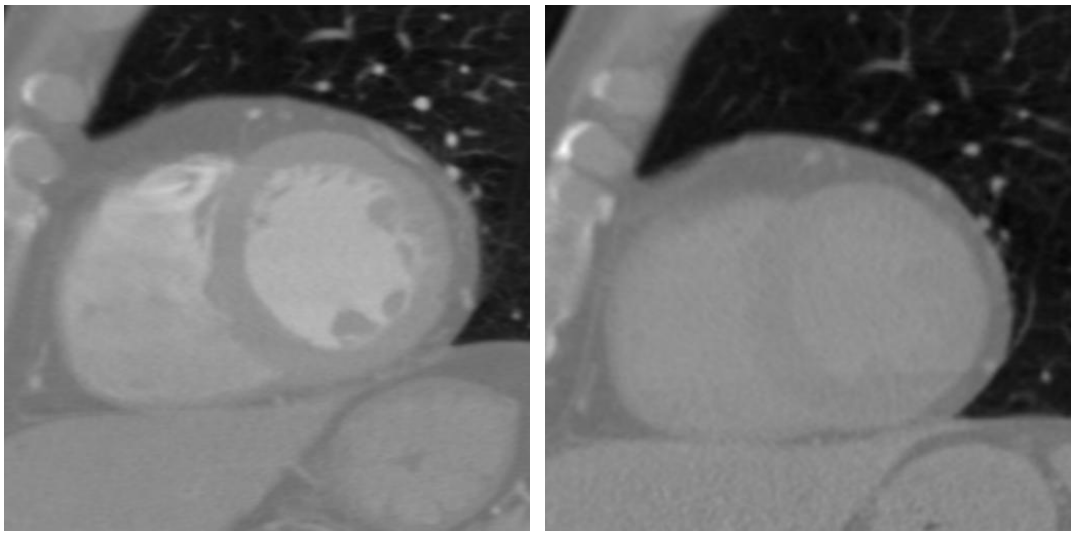

(a) (b)

Fig. 7. The same slice in myocardium MRDCT imaging on (a) artery phase and (b) delayed phase

3.3 Region-Based Myocardium Segmentation

The proposed method automatically estimated the lowest gray-level intensity in the extracted myocardium region of the leading slice. Figure 8 illustrates the initial region of the myocardium of LV in Fig. 1. The inner and outer contours were the endocardium and epicardium boundaries, respectively. The lowest gray-level intensity was different between myocardium and other regions (i.e., the upper right corner region in Fig. 2). After image preprocessing, the distribution of gray-level could count by using the extracted contour of prior slice. By obtaining two peaks with the highest number of pixels from the distribution of gray-level intensity, myocardium and region of fat were differentiated by a predefined threshold T_p which ravine among two peaks (i.e., Otsu's algorithm). Then the result of the mainly myocardium region would be acquired. The extracted myocardium region is shown in Figs. 9(a) and (b).

The region growing method which uses a simple criterion gathers pixels together. In this study, the center myocardium region (i.e., the black of myocardium encircle in Figs. 9(a) and (b)) was utilized as seed of the region growing method to obtain the endocardium region. The method is based on intensity information and chooses adjacent pixels which the pixels have similar intensity. The group of new pixels also chooses adjacent pixels with small rule. Repeat this process until new pixel was joined; the method could obtain a region which has similar intensity. The criterion is described as:

$$I(X) \in (lower, upper), \tag{4}$$

The LV cavity region including seed was segmented beyond the scope of *lower* and *upper*. In this method, the seed was the center of mass in the myocardium.

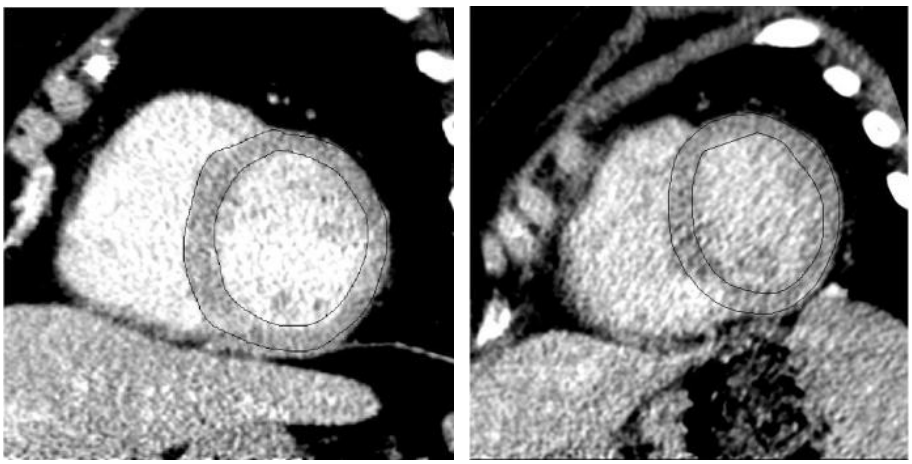

(a) (b)

Fig. 8. The initial region of the myocardium of LV

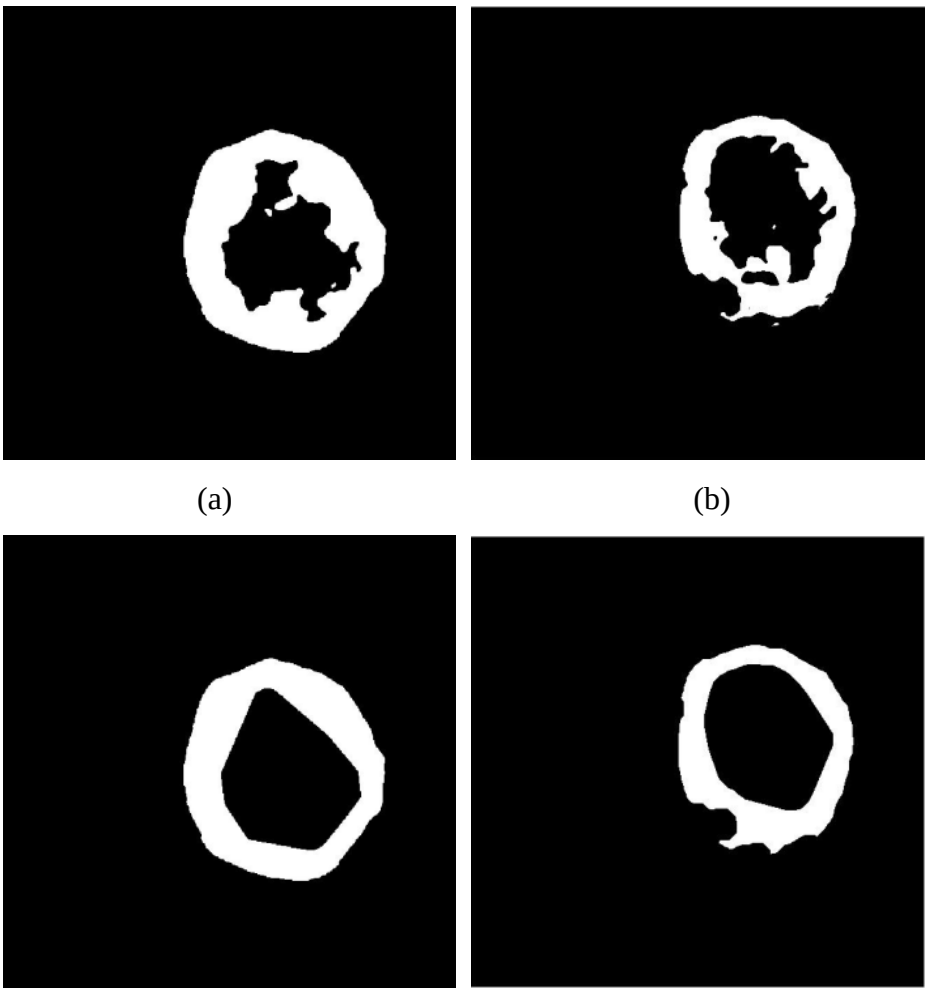

(a) (b)

(c) (d)

Fig. 9. Segmentation results: (a) (b) images after the thresholding method and (c) (d) the region growing segmentations with convex-hull finding algorithm

3.4 Extracted Contour Refinement

Due to incomplete myocardium might occur in few slices of MDCT, an incomplete myocardium would made incorrect result of region growing. Thus the proposed method checked the extracted myocardium region for its completeness before region growing. Figure 10 shows an example of incomplete myocardium segmentation. This problem was solved by using the morphological closing operator. Moreover, the extracted endocardium region might include the papillary muscle area after the thresholding and

region growing procedures. Papillary muscle had similar intensity with LV myocardium, the incorrect segmentation was occurred when the papillary muscle produced spot and connected with the LV myocardium. However, senior physician draws the contour of myocardium that excluded papillary muscle. To achieve the similar result with physician, the convex-hull finding algorithm was utilized to remove the papillary muscle area. The papillary muscle area removed images are shown in Figure 9(c) and (d). The same technique was also used to segment the initial slices in this study.

Width similarity in myocardial region was used to exclude the regions which not belonging to LV myocardium. Base on the width similar characteristic, morphological dilate operator with a spherical structuring element of size 5 was repeated until the expanded region was smaller than 50% of the LV myocardium. Figure 11 shows the final result of extracted myocardium after performing the morphological closing operator. The proposed method also offered an error checking/correction procedure when all slices were segmented. Each slice compared with the corresponding prior slice. When the overlap area of the adjacent slices was smaller than 50%, the error flag was set. Then the interpolation algorithm[17] was employed to generate a new myocardium region to replace the incorrect one to maintain the segmentation accuracy. Termination conditions were employed in Apex slice and Base slice. The termination condition in the Apex was set as that the region of myocardium was disappeared (see Fig. 12(a)). The

termination condition in the Base was set as that the extracted myocardium region was incomplete, as show in Fig. 12(b) and (c).

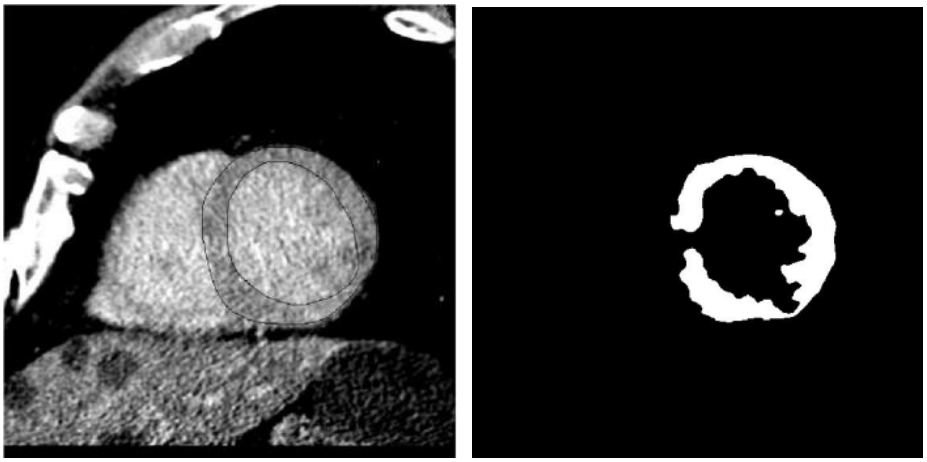

(a) (b)

Fig. 10. Example of an incomplete myocardium segmentation: (a) original image and (b) segmentation result

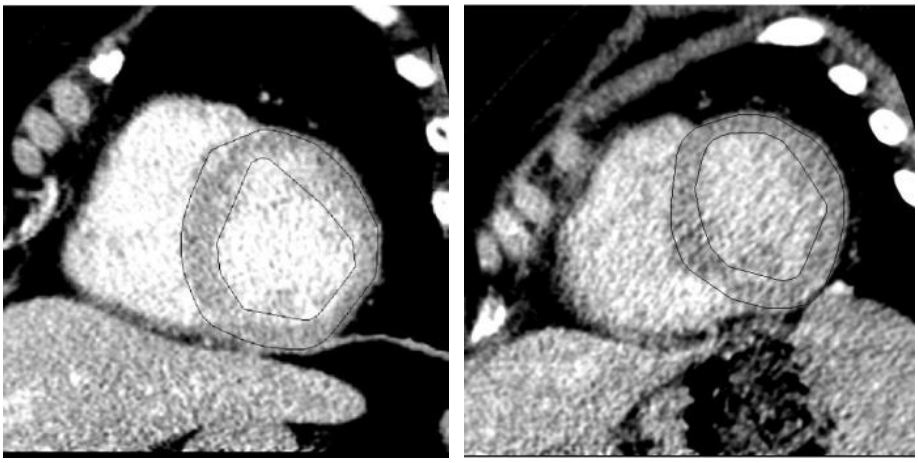

(a) (b)

Fig. 11. Final results of extracted myocardium after performing the morphological closing operator

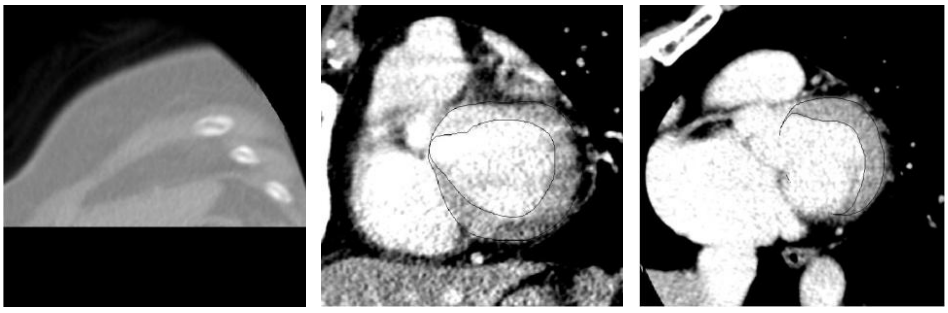

(a) (b) (c)

Fig. 12. Termination condition appearances: (a) imaging in Apex slice and (b)(c) imaging in Base slices

3.5 Completion Validation Checking

Although the full-automatic segmentation always obtained satisfied results, some cases might be failed to find accurate contours due to the position and size of LV myocardium region were not match between the leading slices from delayed phase and artery phase. Hence, a completion validation procedure checked the correctness of the obtained contours from the full-automatic segmentation. In the proposed method, an incorrect segmentation was determined that contouring result by completion criteria. A contouring result was categorized into incorrect segmentation if it conformed to one of the following conditions:

1. The difference of the number of extracted myocardium pixels between delay phase and arterial phase is over 50%.
2. The area of endocardium exceeds 80% of the epicardium area.
3. In the extracted epicardium area, over 1/10 pixels with the intensity which is larger

than the lowest intensity in leading slice.

When the segmentation result was unsatisfied, the semi-automatic segmentation was activated to generate myocardium region of LV.

CHAPTER 4 CONTOUR EVALUATION

This study performed several indices to evaluate the quality of results in quantitative way. Figure 13 demonstrates that contour segmented by the proposed method (*SEG*) and contour segmented by radiologists (*REF*) are overlapped[18]. The term *REF* ∩ SEG denotes the area of *overlap*. The areas of *miss* and *extra* represent segmentation errors of the proposed method. The four indices assessed the similarity between *REG* area and *SEG* area, i.e. similarity index (*SI*), overlap fraction (*OF*), extra fraction (*EF*) and overlap value (*OV*). It means the contour generated by the proposed method is similar to the manual contour, When *SI*, *OF* and *OV* are close to one, and *EF* is close to zero. The indices are defined as:

$$SI = \frac{2 \times (REF \cap SEG)}{REF + SEG}, \tag{5}$$

$$OF = \frac{REF \cap SEG}{REF}, \tag{6}$$

$$OV = \frac{REF \cap SEG}{REF \cup SEG}, \tag{7}$$

$$EF = \frac{\overline{REF} \cap SEG}{REF}. \tag{8}$$

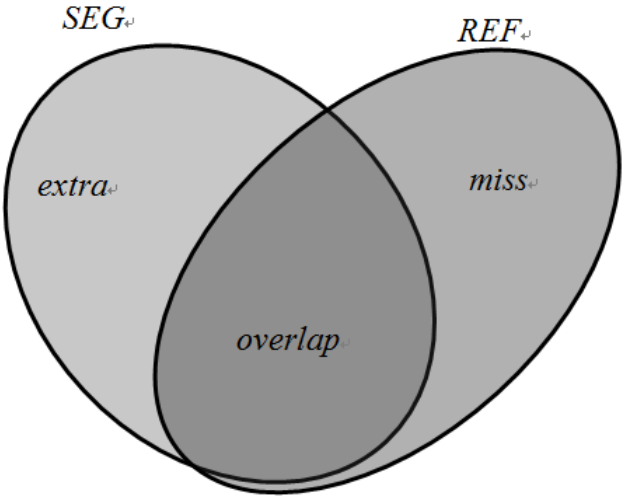

Fig. 13. Comparison of an automated contouring area (*SEG*) with the manual contouring area (*REF*), with (*overlap*) the correctly segmented pixels, (*extra*) the false positives and (*miss*) the false negatives

CHAPTER 5 RESULT

This study assessed the myocardium segmentation method on delayed phase of MDCT imaging. Twenty-seven anonymous healthy patients with finally 326 contours were obtained at the Taichung Veterans General Hospital. For the pre-processing procedure the proposed method set the anisotropic diffusion filter parameters t and k as 30 and 1/7, respectively. In region-based myocardium segmentation phase, the region growing parameters $lower = 0$ and $upper = 0.5$ were set to obtain black region in the binary image. The spherical structuring element with sized 15×15 for the morphological closing operator was used to refine the incompleteness of myocardium. The parameters were supported by the results on experiment. In the simulations, 19 of totally 27 cases obtained satisfied results from the full-automatic segmentation pass of the proposed method. Eight cases were categorized into incorrect segmentation and then got into semi-automatic segmentation pass.

Two experts (denoted Expert#1 and Expert#2) manually delineated contours of left ventricular myocardium individually. Expert#1 is a senior technologist with eight years of experience on cardiac MDCT, Expert#2 is an experienced senior cardiac radiologist with eight years experience. The four similarity measures between the manually determined contours and the automatically detected contours were evaluated.

In the 19 cases (denoted Case#1 to #19) performed the full-automatic segmentation, Table 1 and Table 2 list the average indices of the proposed full-automatic endocardium and epicardium contouring. Figure 14 shows a segmentation result which applied the proposed full-automatic method. For the 8 cases (denoted Case#20 to #27) performed the semi-automatic segmentation, Table 3 and Table 4 list the average indices of the proposed full-automatic endocardium and epicardium contouring. Figure 15 shows a segmentation result which applied the proposed semi-automatic method. The overall performance was listed in Table 5. During proceed with experiment of full-automatic segmentation and semi-automatic segmentation, myocardium segmentation that requires no parameter tuning. Table 6 shows the assessment indices between two expert's manual contours.

All analyses were made on a single CPU Intel Pentium-VI 2Duo 2.33-GHz personal computer with Microsoft Windows XP operating system. The programs were performed using Matlab 2010a software (The MathWorks, Inc., Natick, MA). Average execution time of each case was less than 300 seconds.

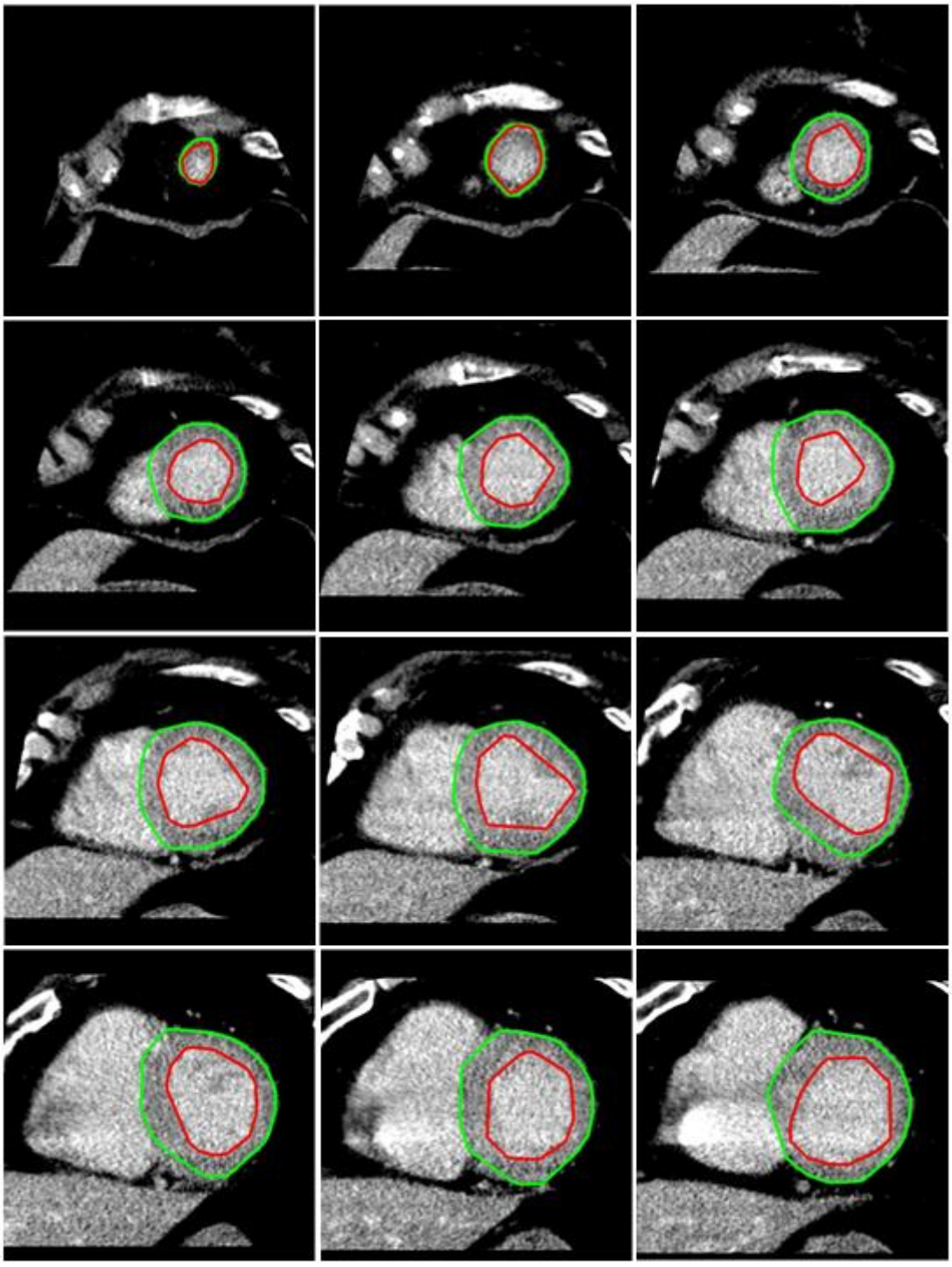

Fig. 14. Contouring results (Case#1) by using the proposed full-automatic method

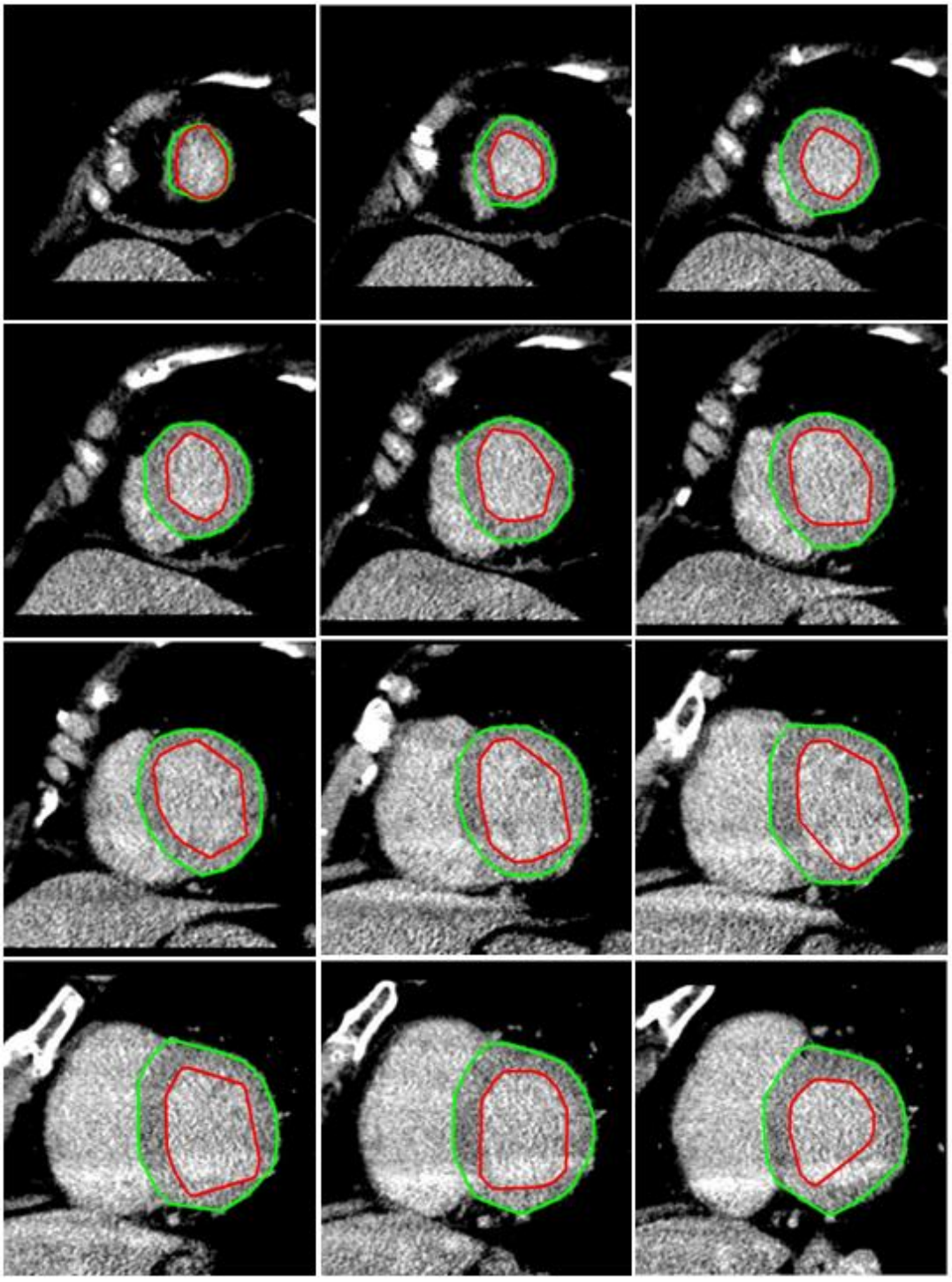

Fig. 15. Contouring results (Case#20) by using the proposed semi-automatic method

Table 1. The contouring evaluations of the proposed full-automatic segmentation which compared with Expert#1 using the measurements

Case#	Endocardium				Epicardium			
	SI	*OF*	*EF*	*OV*	*SI*	*OF*	*EF*	*OV*
1	0.878	0.843	0.213	0.782	0.912	0.921	0.102	0.838
2	0.834	0.852	0.195	0.715	0.912	0.928	0.141	0.837
3	0.847	0.843	0.237	0.735	0.876	0.884	0.013	0.779
4	0.882	0.909	0.231	0.788	0.912	0.922	0.067	0.839
5	0.861	0.895	0.172	0.810	0.904	0.912	0.053	0.825
6	0.815	0.859	0.342	0.688	0.872	0.895	0.081	0.773
7	0.846	0.887	0.241	0.732	0.908	0.915	0.059	0.832
8	0.877	0.912	0.174	0.781	0.914	0.894	0.076	0.842
9	0.834	0.875	0.247	0.715	0.913	0.900	0.053	0.839
10	0.893	0.887	0.194	0.807	0.924	0.915	0.089	0.858
11	0.825	0.859	0.177	0.702	0.913	0.921	0.072	0.840
12	0.824	0.843	0.144	0.701	0.877	0.884	0.059	0.781
13	0.878	0.877	0.111	0.783	0.914	0.930	0.083	0.842
14	0.853	0.874	0.211	0.743	0.825	0.846	0.072	0.702
15	0.852	0.862	0.198	0.743	0.917	0.925	0.049	0.847
16	0.795	0.825	0.323	0.660	0.845	0.856	0.072	0.732
17	0.841	0.857	0.151	0.726	0.854	0.874	0.053	0.745
18	0.839	0.844	0.239	0.723	0.884	0.901	0.091	0.792
19	0.815	0.854	0.284	0.688	0.887	0.894	0.072	0.797
Average	**0.847**	**0.866**	**0.215**	**0.735**	**0.893**	**0.901**	**0.071**	**0.806**

SI : similarity index; *OF*: overlap fraction; *EF*: extra fraction; *OV*: overlap value

Table 2. The contouring evaluations of the proposed full-automatic segmentation which compared with Expert#2 using the measurements

Case#	Endocardium				Epicardium			
	SI	*OF*	*EF*	*OV*	*SI*	*OF*	*EF*	*OV*
1	0.923	0.874	0.224	0.857	0.941	0.952	0.042	0.889
2	0.874	0.899	0.207	0.777	0.931	0.947	0.072	0.870
3	0.847	0.843	0.237	0.735	0.876	0.884	0.013	0.779
4	0.868	0.894	0.337	0.766	0.899	0.925	0.118	0.817
5	0.915	0.924	0.209	0.844	0.930	0.941	0.032	0.870
6	0.902	0.901	0.187	0.822	0.913	0.935	0.053	0.840
7	0.843	0.876	0.324	0.728	0.894	0.934	0.063	0.809
8	0.888	0.918	0.299	0.798	0.933	0.952	0.087	0.874
9	0.899	0.933	0.312	0.817	0.925	0.934	0.063	0.860
10	0.874	0.897	0.225	0.777	0.923	0.938	0.074	0.858
11	0.904	0.907	0.155	0.825	0.941	0.957	0.047	0.889
12	0.886	0.915	0.196	0.795	0.928	0.943	0.055	0.865
13	0.858	0.877	0.187	0.751	0.915	0.925	0.049	0.843
14	0.900	0.937	0.356	0.819	0.936	0.935	0.077	0.880
15	0.886	0.908	0.155	0.796	0.874	0.897	0.081	0.776
16	0.873	0.892	0.150	0.775	0.932	0.946	0.053	0.873
17	0.816	0.836	0.254	0.689	0.885	0.907	0.132	0.794
18	0.847	0.877	0.202	0.734	0.876	0.876	0.052	0.780
19	0.865	0.875	0.198	0.762	0.912	0.927	0.037	0.839
Average	**0.878**	**0.895**	**0.233**	**0.788**	**0.917**	**0.932**	**0.066**	**0.842**

SI : similarity index; *OF*: overlap fraction; *EF*: extra fraction; *OV*: overlap value

Table 3. The contouring evaluations of the proposed semi-automatic segmentation which compared with Expert#1 using the measurements

Case#	Endocardium				Epicardium			
	SI	*OF*	*EF*	*OV*	*SI*	*OF*	*EF*	*OV*
20	0.930	0.927	0.067	0.869	0.966	0.964	0.032	0.934
21	0.902	0.895	0.091	0.821	0.946	0.964	0.075	0.897
22	0.892	0.926	0.151	0.805	0.942	0.973	0.093	0.890
23	0.916	0.978	0.159	0.844	0.960	0.981	0.062	0.923
24	0.915	0.901	0.069	0.843	0.954	0.982	0.077	0.911
25	0.902	0.916	0.114	0.822	0.958	0.963	0.049	0.919
26	0.884	0.932	0.177	0.792	0.963	0.983	0.057	0.929
27	0.901	0.879	0.072	0.820	0.952	0.936	0.031	0.908
Average	**0.905**	**0.919**	**0.113**	**0.827**	**0.955**	**0.968**	**0.060**	**0.914**

SI : similarity index; *OF*: overlap fraction; *EF*: extra fraction; *OV*: overlap value

Table 4. The contouring evaluations of the proposed semi-automatic segmentation which compared with Expert#2 using the measurements

Case#	Endocardium				Epicardium			
	SI	*OF*	*EF*	*OV*	*SI*	*OF*	*EF*	*OV*
20	0.933	0.913	0.045	0.874	0.960	0.966	0.046	0.924
21	0.914	0.945	0.123	0.841	0.960	0.966	0.047	0.923
22	0.891	0.957	0.191	0.804	0.957	0.976	0.062	0.918
23	0.912	0.989	0.180	0.838	0.961	0.976	0.054	0.926
24	0.916	0.916	0.920	0.089	0.956	0.981	0.072	0.915
25	0.897	0.925	0.138	0.813	0.964	0.963	0.036	0.930
26	0.889	0.946	0.182	0.800	0.963	0.977	0.053	0.928
27	0.881	0.860	0.092	0.788	0.952	0.941	0.037	0.908
Average	**0.904**	**0.931**	**0.234**	**0.731**	**0.959**	**0.968**	**0.051**	**0.922**

SI : similarity index; *OF*: overlap fraction; *EF*: extra fraction; *OV*: overlap value

Table 5. The contouring evaluations of the proposed method which compared with the radiologists using the average indices

Compared with	Epicardium				Endocardium			
	SI	*OF*	*EF*	*OV*	*SI*	*OF*	*EF*	*OV*
Expert#1	0.904	0.913	0.070	0.825	0.861	0.894	0.183	0.756
Expert#2	0.925	0.947	0.065	0.861	0.872	0.911	0.211	0.773

SI : similarity index; *OF*: overlap fraction; *EF*: extra fraction; *OV*: overlap value

Table. 6. The contouring evaluations of Expert#2 (set as *SEG*) which compared with Expert#1 (set as *REF*)

Case#	Endocardium				Epicardium			
	SI	*OF*	*EF*	*OV*	*SI*	*OF*	*EF*	*OV*
1	0.941	0.924	0.041	0.888	0.955	0.984	0.077	0.914
2	0.941	0.923	0.039	0.889	0.960	0.985	0.067	0.922
3	0.911	0.874	0.046	0.836	0.951	0.973	0.073	0.907
4	0.891	0.883	0.099	0.803	0.952	0.957	0.054	0.909
5	0.936	0.910	0.034	0.879	0.948	0.976	0.040	0.939
6	0.961	0.960	0.037	0.925	0.971	0.977	0.036	0.943
7	0.932	0.891	0.022	0.872	0.973	0.976	0.032	0.947
8	0.952	0.946	0.042	0.908	0.973	0.972	0.025	0.948
9	0.931	0.941	0.080	0.871	0.962	0.953	0.029	0.926
10	0.956	0.929	0.014	0.916	0.978	0.977	0.020	0.958
11	0.962	0.958	0.034	0.926	0.971	0.964	0.021	0.944
12	0.952	0.959	0.056	0.908	0.974	0.968	0.019	0.950
13	0.946	0.935	0.042	0.898	0.971	0.959	0.016	0.944
14	0.953	0.949	0.042	0.910	0.972	0.957	0.012	0.946
15	0.949	0.931	0.032	0.902	0.974	0.965	0.017	0.949
16	0.946	0.934	0.041	0.897	0.967	0.950	0.015	0.936
17	0.947	0.950	0.056	0.900	0.962	0.966	0.042	0.927
18	0.955	0.961	0.051	0.915	0.974	0.964	0.017	0.948
19	0.908	0.901	0.083	0.832	0.958	0.930	0.011	0.920
20	0.944	0.966	0.082	0.893	0.969	0.962	0.024	0.940
21	0.943	0.936	0.049	0.892	0.972	0.971	0.027	0.945
22	0.933	0.900	0.029	0.875	0.968	0.980	0.046	0.937
23	0.943	0.926	0.037	0.893	0.968	0.981	0.047	0.937
24	0.956	0.937	0.023	0.916	0.973	0.980	0.034	0.948
25	0.941	0.930	0.046	0.889	0.971	0.971	0.029	0.943
26	0.946	0.935	0.043	0.897	0.970	0.975	0.035	0.943
27	0.942	0.948	0.066	0.889	0.971	0.968	0.026	0.943
Average	**0.941**	**0.931**	**0.047**	**0.890**	**0.967**	**0.968**	**0.033**	**0.937**

SI : similarity index; *OF*: overlap fraction; *EF*: extra fraction; *OV*: overlap value

CHAPTER 6 DISCUSSION AND CONCLUSION

Ischemic heart disease could detect by volume of cardiac left ventricle. The volume of cardiac left ventricle was important factor in heart disease diagnosis. This study proposed a segmentation scheme of LV on delayed phase of MDCT. The segmented system was difficult due to myocardial region with each region have similarity intensity, endocardium included papillary muscle, images have noise and determined termination conditions. Therefore, general methods such as level-set, region growing and watershed algorithms hadn't directly applied on delay phase. To conquer these arduous problems, the Otsu, mean shift and convex-hull was used to identify myocardial region in leading slice. Sensible threshold value was found to solve similarity intensity by leading slice sketching (some case by radiologist drawing manually). The proposed method performed convex-hull algorithm to reduce papillary muscle of endocardium, the morphological closing operator and adjustable threshold were used to avoid obtain an incomplete myocardium region. The segmentation results of the proposed method by comparing with manual contours from two experts were 93% and 88% in term of average similarity index, respectively. From the simulations, the proposed method can utilize to assess the more functions for heart disease diagnosis. According to the experiment, the proposed method delineated the contours of LV myocardium accurately and reliably. The inter-observer was 95% in similarity index

with two radiologists. To compare with inter-observer, the result show that obtained that similar with contour from radiologist sketch manually.

In arterial phases and delay phases, dissimilar location and dimension always cause an inaccuracy contouring in the full-automatic segmentation. This study established three conditions to detect the incorrect segmentation. Then the semi-automatic segmentation was activated to generate supplemental myocardium region of LV. However, the unsatisfactory segmentation result was produced in small number cases which were in a low contrast. When the endocardium area was indistinct, both full-automatic and semi-automatic segmentations would fail to contour the desired region. Figure 16 shows an example which had low contrast and blurred myocardium boundary.

This study demonstrated that the performance of the proposed methods to analyze segmentation volume of cardiac left ventricle. The accuracies of the proposed method were 93%, 88% and 89%, respectively. The purpose of this work can be used to analyze diseases of LV from patients by classification and statistical methods. In the future, we will try to improve the performance of full-automatic segmentation and perform the techniques on unhealthy hearts.

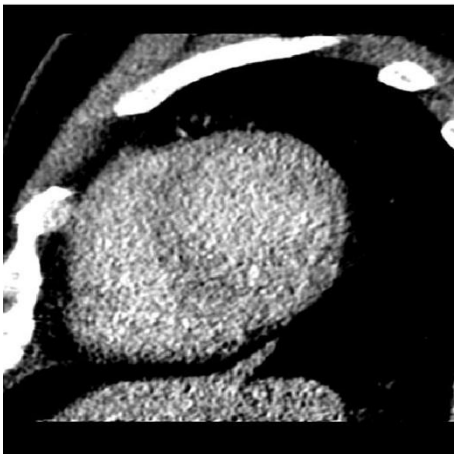

Fig. 16. An example which would fail to obtain satisfactory segmentation

References

[1] I.C. Tsai, W.L. Lee, C.R. Tsao, Y. Chang, M.C. Chen, T. Lee et al., "Comprehensive evaluation of ischemic heart disease using MDCT," *AJR Am. J. Roentgenol.*, vol. 191, no. 1, pp. 64-72, July 2008.

[2] T. Boehm, H. Alkadhi, M. Roffi, J.K. Willmann, L.M. Desbiolles, B. Marincek et al., "Time-effectiveness, observer-dependence, and accuracy of measurements of left ventricular ejection fraction using 4-channel MDCT," *Rofo*, vol. 176, no. 4, pp. 529-537, Apr. 2004.

[3] Y. Zheng, A. Barbu, B. Georgescu, M. Scheuering, and D. Comaniciu, "Four-chamber heart modeling and automatic segmentation for 3-D cardiac CT volumes using marginal space learning and steerable features," *IEEE Trans. Med. Imaging*, vol. 27, no. 11, pp. 1668-1681, Nov. 2008.

[4] Y.L. Huang, Y.R. Jiang, D.R. Chen, and W.K. Moon, "Level set contouring for breast tumor in sonography," *J. Digit. Imaging*, vol. 20, no. 3, pp. 238-247, Sept. 2007.

[5] M. Lynch, O. Ghita, and P.F. Whelan, "Left-ventricle myocardium segmentation using a coupled level-set with a priori knowledge," *Comput. Med. Imaging Graph.*, vol. 30, no. 4, pp. 255-262, June 2006.

[6] J. Dehmeshki, H. Amin, M. Valdivieso, and X. Ye, "Segmentation of pulmonary nodules in thoracic CT scans: a region growing approach," *IEEE Trans. Med. Imaging*, vol. 27, no. 4, pp. 467-480, Apr. 2008.

[7] P.S. Karvelis, A.T. Tzallas, D.I. Fotiadis, and I. Georgiou, "A multichannel watershed-based segmentation method for multispectral chromosome classification," *IEEE Trans. Med. Imaging*, vol. 27, no. 5, pp. 697-708, May 2008.

[8] W.F. Kuo, C.Y. Lin, and Y.N. Sun, "Brain MR images segmentation using statistical ratio: mapping between watershed and competitive Hopfield clustering network algorithms," *Comput. Methods Programs Biomed.*, vol. 91, no. 3, pp. 191-198, Sept. 2008.

[9] J. Zhang, C.H. Yan, C.K. Chui, and S.H. Ong, "Fast segmentation of bone in CT images using 3D adaptive thresholding," *Comput. Biol. Med.*, vol. 40, no. 2, pp. 231-236, Feb. 2010.

[10] J.H. Chen, C.S. Huang, K.C. Chien, E. Takada, W.K. Moon, J.H. Wu et al., "Breast density analysis for whole breast ultrasound images," *Med. Phys.*, vol. 36, no. 11, pp. 4933-4943, Nov. 2009.

[11] M. Park, C.W. Park, M. Park, and C.H. Lee, "Algorithm for detecting human faces based on convex-hull," *Opt. Express*, vol. 10, no. 6, pp. 274-279, Mar. 2002.

[12] R.C. Gonzalez and R.E. Woods, *Digital Image Processing*, second ed. 2001.

[13] W.V. Nicholson and R. Malladi, "Correlation-based methods of automatic particle detection in electron microscopy images with smoothing by anisotropic diffusion," *J. Microsc.*, vol. 213, no. Pt 2, pp. 119-128, Feb. 2004.

[14] I.C. Tsai, Y.L. Huang, and K.H. Kuo, "Left ventricular myocardium segmentation on arterial phase of multi-detector row computed tomography," *Comput. Med. Imaging Graph.*, Apr. 2011.

[15] L.G. Wang, C. Zheng, L.Y. Lin, R.Y. Chen, and T.C. Mei, "[Fast segmentation algorithm of high resolution remote sensing image based on multiscale mean shift]," *Guang. Pu. Xue. Yu Guang. Pu. Fen. Xi.*, vol. 31, no. 1, pp. 177-183, Jan. 2011.

[16] N. Otsu, "A threshold selection method from gray-level histograms," *IEEE Trans. Syst. Man Cybern*, vol. 62-66 1979.

[17] Q. Huang, Y. Zheng, M. Lu, T. Wang, and S. Chen, "A new adaptive interpolation algorithm for 3D ultrasound imaging with speckle reduction and edge preservation," *Comput. Med. Imaging Graph.*, vol. 33, no. 2, pp. 100-110, Mar. 2009.

[18] P. Anbeek, K.L. Vincken, M.J. van Osch, R.H. Bisschops, and G.J. van der, "Probabilistic segmentation of white matter lesions in MR imaging," *Neuroimage.*, vol. 21, no. 3, pp. 1037-1044, Mar. 2004.